Comparison of Classic and Generalized Intersection Approach for the Synthesis of Transmitarrays with Near-field Constraints

Sergio M. Feito
Dept. Electrical Engineering
Universidad de Oviedo
Gijón, Spain
menendezfsergio@uniovi.es

Álvaro F. Vaquero
Dept. Electrical Engineering
Universidad de Oviedo Gijón, Spain
Instituto de Telecomunicações (IT)
Lisbon, Portugal

Francesco Foglia Manzillo
CEA – Leti,
Univ. Grenoble-Alpes
F-38000 Grenoble, France

Antonio Clemente
CEA – Leti,
Univ. Grenoble-Alpes
F-38000 Grenoble, France

Manuel Arrebola
Dept. Electrical Engineering
Universidad de Oviedo
Gijón, Spain

***Abstract*— In this work, two different methods based on the Intersection Approach (IA) for the synthesis of transmitarrays are compared. The first method leverages the Fast Fourier Transform (FFT) to efficiently seek solutions when constraints are enforced only on planes parallel to the radiating aperture. The second method aims to overcome the limitations of the first one in terms of generality, using a different model for the near-field computation and an alternative algorithm for the backward operator. To benchmark the two methods, the synthesis of a relatively large (576 elements) Ka-band transmitarray with a shaped near-field pattern is performed. The results reveal certain advantages and disadvantages for each method. The classic IA demonstrates faster convergence to a solution due the reduced computational complexity of the FFT. Conversely, the generalized IA yields slightly better fulfillment of the imposed requirements. Importantly, both solutions closely align with the challenging objectives of the synthesis.**

Keywords—Transmitarray, Intersection Approach, Near Field Synthesis.

I. Introduction

The analysis and synthesis of near-field antennas have attracted increasing interest in a range of applications, including wireless power transfer [1], medical scanners and hyperthermia treatments [2], and next-generation smart access points [3]. These applications often require precise shaping of the radiated near field (NF) in specific planes or volumes [4].

Transmissive and reflective spatially fed arrays (SFAs), such as transmitarrays (TAs) and reflectarray (RA) antennas, have emerged as effective solutions for controlling the radiated field amplitude in the Fresnel zone of the antenna. Unlike conventional phased arrays, SFAs can achieve high radiation efficiency even in the millimeter-wave (mm-wave) band, as they do not require complex feeding networks, even when the radiating aperture is electrically large. Among SFAs, TAs offer several advantages over RAs, as it does not require offset-feed configurations and nor exhibit feed blockage. A TA is a quasi-periodic structure composed of unit cells (UCs) that introduce a local phase delay to the incident field provided by the primary feed, thereby re-radiating it. By carefully designing the UCs and tailoring the phase-shift distribution over the TA surface, the near-field pattern can be precisely shaped.

The optimization of the phase-shift distribution is usually performed by array synthesis techniques. Several methods have been proposed for SFAs in recent years. Among others, the Intersection Approach (IA) (an alternate projection method) has been successfully employed for the synthesis of SFAs [5] [6]. However, most works address far-field shaping. Indeed, the original classic IA algorithm allow one to compute the far field and retrieve the corresponding source field on the array surface using basic Fourier analysis. When dealing with the near-field synthesis, the FFT cannot be directly used, and both forward and backward operators must be redefined.

This work aims to fairly compare two different phase-only synthesis techniques for shaping the near field emitted by a TA. The first method uses a classic IA, while the second one uses a generalized version (gIA) [6]. They differ for the models used to compute both the forward (propagation) and backward (projection) operators. The classic IA exploits Fourier analysis to efficiently calculate the field on planes parallel to the TAs, via FFTs. The proposed gIA is more general, as it computes the near field in any point, by superposition of the far fields radiated by each UC and uses the Levenberg–Marquardt algorithm [7] to optimize it.

II. Synthesis Models using IA

A. Intersection Approach

The IA considers two sets: the set $\mathcal{M}$ of the radiated fields that fulfill the requirements, and the set $\mathcal{R}$ of the feasible radiated fields, i.e. the fields that can be physically radiated by the antenna [5]. The search for the intersection between these two sets is an iterative process based on the method of Alternate Projections. The latter one performs two operations at each iteration, which can be mathematically expressed as:

$$E_{NF}^{i+1} = \mathcal{B}\left[\mathcal{F}\left(E_{NF}^{i}\right)\right], \tag{1}$$

where E_{NF}^{i} is a component of the NF radiated by the TA at the i^{th}-iteration, $\mathcal{F}$ is the forward projection operator, which projects a point of $\mathcal{R}$ onto $\mathcal{M}$, and $\mathcal{B}$ is the backward projection operator, which projects a point of $\mathcal{M}$ onto $\mathcal{R}$.

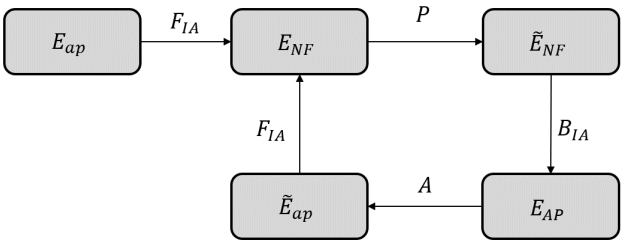

Fig. 1. Flowchart of the classic Intersection Approach algorithm.

The framework can be easily translated into field components to relate the tangential fields over the TA aperture ($\vec{E}_{AP}$) with the field radiated by them ($\vec{E}_{NF}$).

$$\vec{E}_{AP}(x_m, y_n) = \boldsymbol{T}^{mn} \cdot \vec{E}_{inc}(x_m, y_n) \tag{2}$$

where $\boldsymbol{T}^{mn}$ is the transmission coefficient matrix that relates the complex amplitude of the tangential components of the incident field ($\vec{E}_{inc}(x_m, y_n)$) and the transmitted electric field by the mn^{th} element of the TA located at the point (x_m, y_n). It can be expressed as:

$$\boldsymbol{T}^{mn} = \begin{pmatrix} \Gamma_{xx}^{mn} & \Gamma_{xy}^{mn} \\ \Gamma_{yx}^{mn} & \Gamma_{yy}^{mn} \end{pmatrix} \tag{3}$$

Due to the physical characteristics of the TA structure, the synthesis procedure will be a phase-only synthesis (POS), because the incident amplitude is fixed and determined by both the configuration and the antenna selected as the primary feed. For simplicity, the behavior of the elements comprising the TA will be considered ideal phase shifters, therefore the element will only introduce a phase delay and no losses. These two considerations combined with the assumption that there is no cross-polarization, lead to a simplified form for $\boldsymbol{T}^{mn}$.

$$\boldsymbol{T}^{mn} = \begin{pmatrix} e^{j\angle\Gamma_{xx}^{mn}} & 0 \\ 0 & e^{j\angle\Gamma_{yy}^{mn}} \end{pmatrix} \tag{4}$$

Looking at the flowchart of the classic IA algorithm illustrated in Fig. 1 the near field can be computed using the forward propagator F_{IA} and the aperture field of a certain radiated near field can be retrieved using B_{IA}. These operators' definition will make the difference between both algorithms the that will be introduced in following sections.

Once the field at the aperture is computed, the near field (E_{NF}) can be obtained by forward propagation. This computed near field will typically not fulfill the constraints. Thus, additional operations (P) are performed to obtain a field in $\mathcal{M}$. To this end, two masks (T_{upper} and T_{lower}) describing the maximum and minimum acceptable field values, for each spatial point, are described. In both methods presented in this work, a modified near field ($\tilde{E}_{NF}$) falling in the $\mathcal{M}$ set is then defined as:

$$\tilde{E}_{NF} = \begin{cases} T_{upper}\,; & if\ |E_{NF}| \geq T_{upper} \\ T_{lower}\,; & if\ |E_{NF}| \leq T_{lower} \\ E_{NF}\,; & otherwise \end{cases} \tag{5}$$

However, this modified field is not necessarily feasible, since the constraints are only imposed on the radiated field but not on the aperture field. Thus, backpropagating this field is again not enough to ensure that the retrieved aperture field (E_{AP}) falls into $\mathcal{R}$. Therefore, the synthesis procedure requires one more step (A) to obtain a TA aperture field ($\tilde{E}_{AP}$) that can be physically realized using the selected primary feed and antenna optics.

B. Classic IA

In the classic implementation of IA, both forward and backward projectors are based on the use of FFT. However, when dealing with near-field implementation some modifications and constraints should be introduced to get a proper simple model.

In particular, the region of validity of the model calculating the field radiated by the antenna is restricted to planes parallel to the aperture of the antenna, provided the TA aperture is also planar. Under these assumptions, the forward propagator (F_{IA}) is defined as:

$$E_{NF}(x, y, z_0) = \frac{1}{4\pi^2}\mathfrak{F}^{-1}\{g_p \mathfrak{F}\{E_{AP}(x, y)\}\} \tag{6}$$

where $\mathfrak{F}$ and $\mathfrak{F}^{-1}$ are the operators for direct and inverse Fourier transforms, respectively. It is assumed that the aperture field has only one non-zero component (E_{AP}). The factor $g_p = e^{-jk_z z_0}$ [8] represents a spatial translation by z_0 along the z-axis, where k_z is the z-component of the wave vector, given by:

$$k_z = \begin{cases} \sqrt{k_0^2 - k_x^2 - k_y^2}\,, & k_0^2 \geq k_x^2 + k_y^2 \\ -j\sqrt{-k_0^2 + k_x^2 + k_y^2}\,, & k_0^2 < k_x^2 + k_y^2 \end{cases}, \tag{7}$$

being k_0 the free-space propagation constant, k_x and k_y the spatial frequencies extending over the entire spectrum.

Combining this propagator with the previously defined operator P described by (5), the forward projector $\mathcal{F}_{IA}$ is completely defined.

In a similar way, the backward propagator (B_{IA}) can be expressed as follows:

$$E_{AP}(x, y) = \frac{1}{4\pi^2}\mathfrak{F}^{-1}\left\{g_b \mathfrak{F}\{\tilde{E}_{NF}(x, y, z_0)\}\right\}, \tag{8}$$

where $g_b = e^{jk_z h z_0}$. The expression for k_z is similar to that in (7). However, when the second condition ($k_0^2 < k_x^2 + k_y^2$) is met, the positive imaginary root is retained.

At this point, following the diagram depicted in Fig. 1, only operator A is missing to have the complete procedure. As mentioned in the previous section, the amplitude of the field on the TA aperture is dependent on the incident field, so it cannot be ensured E_{AP} is a feasible tangential field. Only the phase of E_{AP} can be adjusted by distributing the UCs in the TA. Therefore, the following feasible aperture field ($\tilde{E}_{AP}$) is prescribed, after the backward propagation, to be used in the next iteration of the algorithm:

$$\tilde{E}_{AP} = \begin{cases} |E_{inc}| e^{j\angle E_{AP}}\,; & |x| \leq \frac{D_x}{2}\,, |y| \leq \frac{D_y}{2} \\ 0\,; & otherwise \end{cases}, \tag{9}$$

where D_x and D_y are the dimensions of the TA aperture in x and y dimensions respectively (see Fig. 3).

Both the forward ($\mathcal{F}_{IA}$) and backward ($\mathcal{B}_{IA}$) projectors are defined now and by iterating the procedure presented in (1), a

solution that satisfies both the physical constraints on the aperture field and the near-field pattern constraints may be found.

C. Generalized IA

In this generalized version, the forward propagator (F_{gIA}) is defined using the principle of superposition, whereby each element of the transmitarray (TA) is considered as a radiating element modelled as a small aperture antenna. This allows for the calculation of the near-field radiation pattern produced by the TA at any given point in space by summing up the far-field contributions from each cell of the TA, i.e. as:

$$E_{NF}(x,y,z) = \sum_{m=1}^{M} E_{FF}^{m}(x,y,z) \tag{10}$$

where (x,y,z) is the point where the near field of the TA is computed, M is the total number of UCs, and $E_{FF}^{m}(x,y,z)$ is the far field radiated by the m-th element at the desired point. The far-field contribution of the m -th element can be computed using the second principle of equivalence for planar aperture antennas [10].

Combining this forward propagator with the previously defined operator T in (5), the forward projection operator $\mathcal{F}_{gIA}$ is completely defined for the gIA implementation.

In the classic IA, the most challenging aspect is the backward projector, specifically the definition of an operator B_{gIA} not restricting the region where the synthesis can be performed. An alternative approach consists in using an optimization algorithm [9]. In this case, the Levenberg–Marquardt algorithm (LMA) has been selected for integration within the Intersection Approach (IA).

In order to use the LMA in the generalized Intersection Approach, a functional, denoted as d, is introduced. This functional evaluates the distances between points in set $\mathcal{R}$ and points in set $\mathcal{M}$, thereby measuring the discrepancy between the desired near-field distribution (E_{NF}) and the synthesized near-field distribution ($\tilde{E}_{NF}$) (as depicted in Fig. 2). The functional is based on the Euclidean distance concept, but it is important to note that each element in these sets must be expressed in terms of both magnitude and phase. Therefore, the functional takes into account the magnitude and phase distances independently to accurately assess the discrepancy between the desired and synthesized near-field patterns.

$$d = \int_{\Omega} w_M \left(\left| \tilde{E}_{NF} \right|^2 - |E_{NF}^{LMA}|^2 \right) d\Omega + \int_{\Omega} w_P \left(\angle \tilde{E}_{NF} - \angle E_{NF}^{LMA} \right) d\Omega, \tag{11}$$

where Ω is the volume where the near field is computed and w_M and w_P are weight functions.

III. Near Field Shaped TA

A. TA optics

The structure used in order to compare both presented synthesis procedures is a square 24×24 (576) elements, which are distributed in a regular grid of a periodicity of $\lambda/2 \times \lambda/2$ along the x- and y-axes.

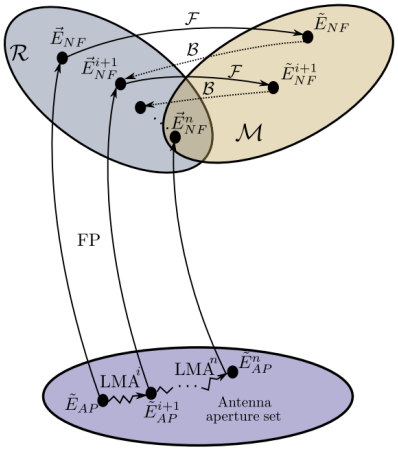

Fig. 2. Schematic diagram illustrating the generalized Intersection Approach iterative process. Extracted from [6].

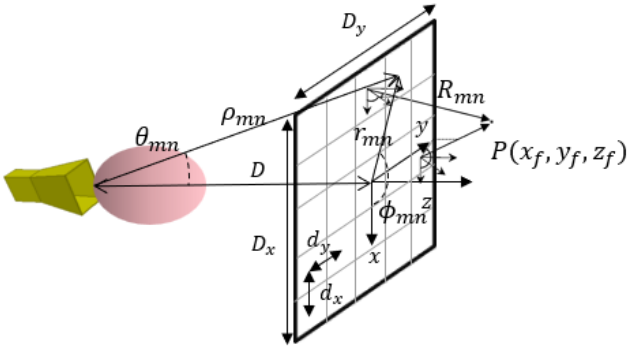

Fig. 3. Sketch of the transmitarray geometry.

In this case, the TA is fed using a pyramidal horn of 10 dBi gain, located at a distance (D in Fig. 3) of 0.1 m and aligned with the center of the lens. The feed generates an illumination taper of -19.7 dB at the edge of the TA, at the working frequency of 30 GHz.

The TA synthesis aims to obtain a flat top beam at a distance of 22λ with a -3dB spot of $11\lambda\,(x) \times 5\lambda\,(y)$, i.e. $(0.11\text{ m} \times 0.05\text{ m})$, maintaining the SLLs below -12dB. Additionally, a maximum ripple of 1 dB is required in the flat-top region.

Considering the geometry described above, the starting phase profile of the TA is selected to just compensate for the different phase delays in the incident field. Thus, the radiated field that will be the seed of both methods is a far-field focused pencil beam.

B. Near-field synthesis results

The optimization process has not been divided into different stages. Although this may result in poor convergence, it is useful to test both algorithms in a non-ideal environment to assess their robustness.

The results obtained for both principal cuts using both methods are shown in Fig. 5. Both synthesis procedures quickly converged to feasible solutions. Upon closer examination of the results, it is evident that the requirements were mostly achieved in both cases, fulfilling the masks in around a 98% for the gIA and a 97% for classic implementation of the points where it was enforced Both methods fulfilled the -3 dB spot requirements, yielding an

approximate result of $(0.12(x) \times 0.05(y)\ m)$ in both cases. The SLL requirement was also largely met, and the ripple obtained in the flat-top regions was nearly equal, with an approximate value of -0.6 dB.

The classic IA implementation managed to converge to the phase profile shown in Fig. 4 (a) in just about 4 seconds thanks to the use of FFT. In contrast, the generalized IA required approximately 9 minutes to converge to the phase profile in Fig. 4 (b). This was expected since the generalized approach computes the near field as a sum rather than using an FFT and runs the LMA. Additionally, the selected TA consists of a significant number of UCs (576 elements), which further amplifies the differences in computational cost.

Moreover, it appears that the generalized IA is less prone to getting stuck in local solutions, as the solution returned by the synthesis procedure slightly better satisfies the requirements compared to the classic IA. However, the phase profile generated by the classic IA synthesis exhibits smoother spatial variations than that obtained with the generalized IA.

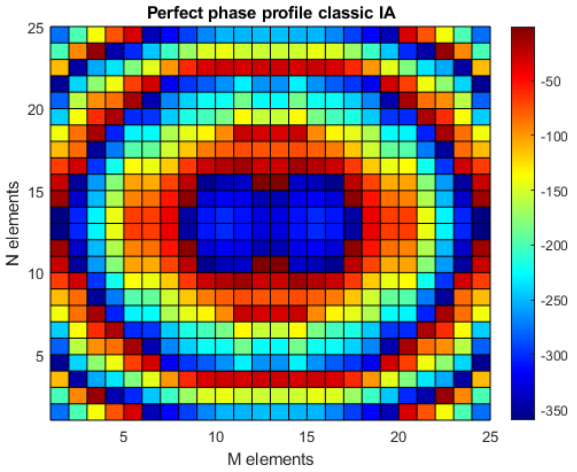

(a)

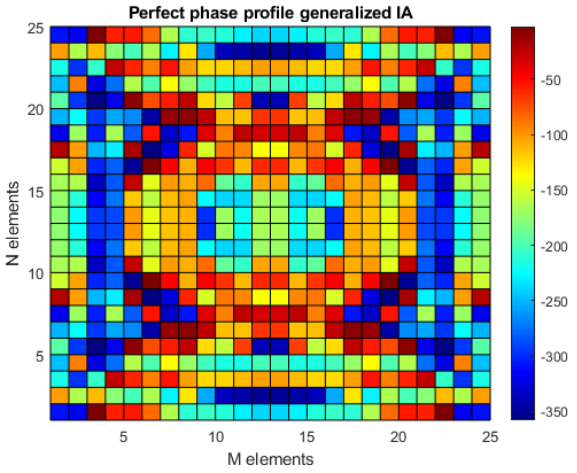

(b)

Fig. 4. Phase profile in degrees obtained after the optimization process for the 24×24 near field shaped TA: (a) using the classic IA; (b) using the generalized IA.

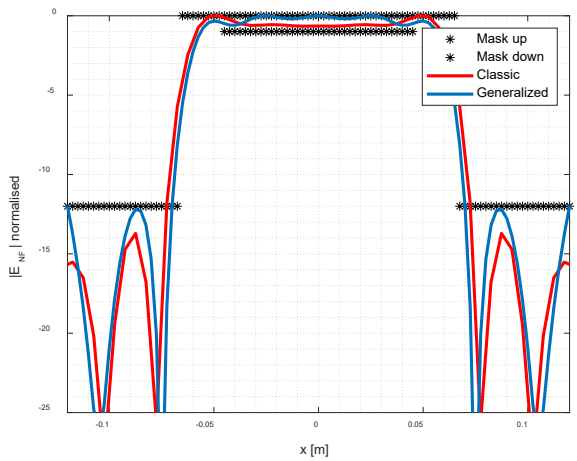

(a)

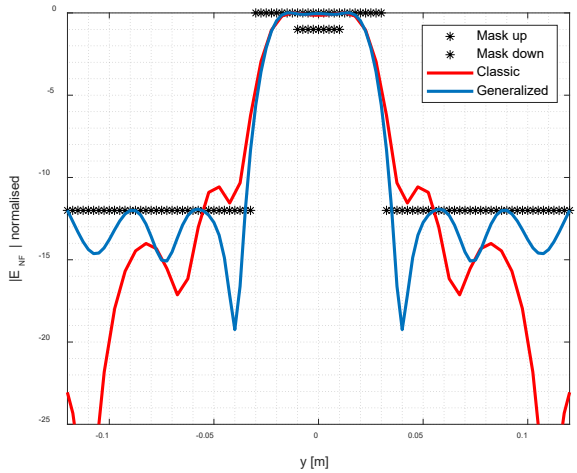

(b)

Fig. 5. Comparison of the normalized NF amplitude cuts obtained performing the TA phase-only synthesis (24×24 elements) with the classic IA and the generalized IA, respectively. (a) Vertical cut along x (see Fig. 3) and (b) horizontal cut along y (see Fig. 3), at a distance of 22 λ from the radiating aperture.

IV. Conclusion

In this work, two different methods for the phase-only synthesis of TAs have been introduced. Both techniques are based on the IA but differ for the models used to compute the near field and the techniques to retrieve the aperture field. The first, the classic IA, uses the FFT to rapidly converge, but can be used only when the field constraints are enforced on planes parallel to the TA. The second one, the generalized IA, avoids the limitations of the back propagation step of the previous one, using the LMA optimization, and allows one to shape the field emitted by a TA in an arbitrary set of point in its Fresnel region.

The two methods have been benchmarked discussing the synthesis of a relatively large (24×24 elements) Ka-band transmitarray with a shaped near-field pattern. The capability of both optimization techniques to escape local minima has been evaluated using the same seed and enforcing several stringent constraints. Moreover, the feasibility of the obtained solutions in terms of physical implementation, e.g., the smoothness of the phase variation over the TA, the

compliance with the target pattern, and the computation time have been compared.

The results of our analysis demonstrate that the classic IA method exhibits faster convergence. On the other hand, the generalized IA method yields a solution that slightly better meets the imposed requirements.

Overall, this study highlights the potential benefits of employing computational enhancement methods, such as FFT, when the pattern requirements are prescribed only on planes parallel to the TA. Both methods demonstrate a strong agreement with the objectives of the synthesis, highlighting their suitability for transmitarray design and optimization.

ACKNOWLEDGMENT

This work has been supported in part by MCIN/AEI/10.13039/501100011033 within the projects PID2020-114172RB-C21 and TED2021-130650B-C22, the Spanish Ministry of Universities and European Union (NextGenerationEU fund) under project MU-21-UP2021-03071895621J, and by the Gobierno del Principado de Asturias under project AYUD/2021/51706.

REFERENCES

[1] A. Razavi, R. Maaskant, J. Yang, and M. Viberg, “Optimal aperture Distribution for near-field detection of foreign objects in lossy media,” in *Proc. IEEE-APS Topical Conf. Antennas Propag. Wireless Comm.*, Palm Beach, Aruba, 2014, pp. 659–662.

[2] X. He, W. Geyi, and S. Wang, “Optimal design of focused arrays for microwave-induced hyperthermia,” *IET Microw., Antennas Propag.*, vol. 9, no. 14, pp. 1605–1611, 2015.

[3] A. Buffi, A. A. Serra, P. Nepa, H. T. Chou, and G. Manara, “A focused planar microstrip array for 2.4 GHz RFID readers,” *IEEE Trans. Antennas Propag.*, vol. 58, no. 5, pp. 1536–1544, Mar. 2010.

[4] I. Iliopoulos *et al*, "3-D Shaping of a Focused Aperture in the Near Field," *IEEE Trans. Antennas Propag.*, vol. 64, no. 12, pp. 5262-5271, Dec. 2016.

[5] J. A. Zornoza and J. A. Encinar, “Efficient phase-only synthesis of contoured-beam patterns for very large reflectarrays,” *Int. J. RF Microw. Comput. Eng.*, vol. 14, no. 5, pp. 415–423, Sep. 2004.

[6] Á. F. Vaquero et al. "Demonstration of a reflectarray with near-field amplitude and phase constraints as compact antenna test range probe for 5G new radio devices," *IEEE Trans Antenna Propag.*, vol. 69, no. 5, pp. 2715-2726, May 2021.

[7] J. Nocedal and S. J. Wright, Numerical Optimization, Springer, 2nd edition, 2006.

[8] J. E. Hansen, *Spherical near-field antenna measurements*, 1988.

[9] O. M. Bucci, G. D’Elia, G. Mazzarella, and G. Panariello, “Antenna pattern synthesis: a new general approach,” *Proc. IEEE*, vol. 82, no. 3, pp. 358–371, Mar. 1994.

[10] C. A. Balanis, Antenna theory: analysis and design, 3rd Ed. Hoboken, NJ, USA: Wiley Interscience, 2005.

[11] Á. F. Vaquero, M. R. Pino, M. Arrebola, S. A. Matos, J. R. Costa and C. A. Fernandes, "Bessel beam generation using dielectric planar lenses at millimeter frequencies," *IEEE Access*, vol. 8, pp. 216185-216196, 2020.